some new work "in the field lying between organic and inorganic chemistry, and perhaps involving the newer but less fanciful ideas of valency" (W. H. Carothers to J. R. Johnson, 21 September 1936, Acc. 1842). He never seemed to be able to get going, though. The death of his sister, Isabel Carothers Berolzheimer on 7 January 1937, dealt him a severe blow from which he never recovered [see R. Adams in (*11*)]. The date of her death is erroneously listed as 1936. Her obituary was in the *New York Times* of 9 January 1937. What precipitated Carothers's suicide is not known. His obituary was in the *Wilmington Journal Every Evening* on 30 April 1937.

38. Carothers's obsession that he was a failure has been noted by many of his friends and associates. His psychiatrist in Philadelphia concurred in this assessment. I. H. Carothers to R. Adams, 2 December 1937, Adams Papers, Box 54, UILA.
39. See E. K. Bolton, interview, in (*34*); R. Adams to F. Woodward, 8 November 1934, in (*9*).
40. See L. Wise and N. Fisher in (*22*), pp. 15–17.
41. We thank the members of our Du Pont and Academic Advisory Committees for their criticism. Thanks also to L. B. Gortler.

RESEARCH ARTICLE

Mainbelt Asteroids: Dual-Polarization Radar Observations

Steven J. Ostro, Donald B. Campbell, Irwin I. Shapiro

Abstract. *Observations of 20 asteroids in the main belt between Mars and Jupiter provide information about the nature of these objects' surfaces at centimeter-to-kilometer scales. At least one asteroid (Pallas) is extremely smooth at centimeter-to-meter scales. Each asteroid appears much rougher than the Moon at some scale between several meters and many kilometers. The range of asteroid radar albedos is very broad and implies substantial variations in porosity or metal concentration (or both). The highest albedo estimate, for the asteroid Psyche, is consistent with a surface having porosities typical of lunar soil and a composition nearly entirely metallic.*

Asteroids comprise an enormous, variegated population of solid bodies and new information concerning them is essential to our understanding of the origin and evolution of the solar system. They may be examples of the first material to accrete from condensates in the solar nebula that existed about 4.6 billion years ago, but some asteroids apparently have undergone varying degrees of chemical differentiation, geologic evolution, and collisional modification. Apart from their scientific significance, asteroids also have economic potential as sources of water, organic compounds, and free metal for the industrialization in space envisioned for the next century.

During the last decade, the number of catalogued asteroids has grown from 2000 to more than 3200, and physical studies of these diminutive objects have expanded dramatically. Observations in the visible and infrared (VIS/IR) parts of the spectrum have demonstrated that the distributions of asteroid sizes and rotation periods span several orders of magnitude and suggest that the compositional diversity of asteroids exceeds that of our meteorite sample. However, asteroids generally cannot be resolved by ground-based optical telescopes and have yet to be examined by spacecraft; and therefore, with very few exceptions, their fundamental physical properties remain poorly known.

Radar observations can provide spatial resolution of a target in a manner that is independent of the target's apparent angular size and, because of the radio wavelengths employed, can also provide information about surface structure at scales much larger than those probed optically but still much smaller than typical asteroid dimensions. During the 12 years after the first radar detection of an asteroid (in 1968), the potential contributions of radar observations of asteroids were realized most fully for the Earth-approaching objects 433 Eros (*1*) and 1685 Toro (*2*). But until 1980, the high signal-to-noise ratios and dual-polarization measurements that yielded useful information about these objects' physical properties were not available for asteroids in the main belt between Mars and Jupiter.

Here we discuss results of 13-cm wavelength, dual-polarization radar observations of 20 mainbelt asteroids, conducted at the Arecibo Observatory in Puerto Rico during 1980 to 1985. Our measurements provide information on asteroid surface characteristics at scales between several centimeters and several kilometers, and also furnish unique constraints on surface bulk density and metal concentration, neither of which is tightly constrained by optical methods.

Observations. Table 1 lists each target's geocentric coordinates for a convenient epoch near the weighted midpoint of the observation dates. Radar system characteristics and our observational, data-acquisition, and data-reduction techniques were nearly identical to those described in (*2*). Echo power spectra were obtained in the same rotational sense of circular polarization as transmitted (that is, the SC sense) as well as in the opposite (OC) sense. Since the handedness of a circularly polarized wave is reversed on normal reflection from a smooth dielectric interface, the OC sense dominates echoes from planetary surfaces that look smooth at the observing wavelength, λ. (A single dielectric interface with minimum radius of curvature $>> \lambda$ would look smooth.) The presence of an SC component can be caused by multiple scattering from smooth interfaces or by reflections from interfaces that are rough at small ($\sim\lambda$) scales. The ratio of SC to OC echo power is thus a useful indicator of near-surface, small-scale "roughness."

Each of our spectra consists of ~400 independent estimates of echo power density at frequency intervals of Δf Hz (Table 1). Figure 1 shows weighted-mean OC and SC echo spectra for our 15 targets with the strongest echoes. Table 1 lists estimates of the OC radar cross section, σ_{oc}, obtained by integrating the power spectra, and of the circular polarization ratio, $\mu_c \equiv \sigma_{sc}/\sigma_{oc}$ (*3*).

Polarization ratio: Small-scale structure. For each asteroid, most of the echo

Steven J. Ostro is a member of the Technical Staff at the Jet Propulsion Laboratory, California Institute of Technology, Mail Stop 183-501, 4800 Oak Grove Drive, Pasadena 91109. Donald B. Campbell is director of operations of the National Astronomy and Ionosphere Center, Box 995, Arecibo, Puerto Rico 00613. Irwin I. Shapiro is director of the Harvard-Smithsonian Center for Astrophysics, 60 Garden Street, Cambridge, Massachusetts 02138.

power is in the OC polarization. Estimates of μ_c range from 0.00 to 0.40 and have an unweighted mean and rms dispersion of 0.12 ± 0.10. This mean λ13-cm circular polarization ratio is similar to the λ23-cm value (~0.1) measured for the Moon (*4*), and therefore we do not expect extreme differences between lunar and typical mainbelt asteroidal decimeter-scale morphologies.

The lowest values of μ_c (for example, 0.05 ± 0.02 for the asteroid 2 Pallas) require that nearly all the echo must be due to single-reflection backscattering from surface elements that are very smooth at all scales within about an order of magnitude of the wavelength. The asteroids we observed are thought to be large enough to be covered by regoliths, that is, layers of loose, porous, particulate debris, generated by impacts and having thicknesses $\gtrsim$1 km (*5*). Pallas's minute value of μ_c requires the virtual absence of centimeter-to-meter-scale structure within the top several meters of regolith. At the opposite extreme, the largest values of μ_c (for example, 0.40 ± 0.11 for 4 Vesta and 0.25 ± 0.05 for 80 Sappho) reveal substantial decimeter-scale structure near the surface. However, even for these targets, much of the echo must arise from single reflections from smooth surface elements.

In Fig. 2a we plot estimates of μ_c as a function of asteroid diameter (Table 1). The plotting symbols indicate each asteroid's taxonomic type (C, S, M, P, or V) as assigned by (*6*). In constructing this taxonomy, the visual albedos and 0.3- to 1.3-μm spectral reflectances of several hundred asteroids were subjected to cluster analysis. The resultant clusters are thought to correspond to different mineralogical compositions (*7*). For example, C and P types are thought to have surfaces that are mineralogically similar to carbonaceous chondritic meteorites. Possible meteoritic analogues for S types are ordinary chondrites and stony irons, and possible meteoritic analogues for M types are enstatite chondrites and irons. The V designation is reserved for Vesta, whose unique VIS/IR spectrum resembles those of some basaltic achondrites.

The C and S types dominate the main belt between 2.0 and 3.0 astronomical units (AU), and also constitute most of our radar sample. The unweighted mean and rms dispersion of μ_c for the C and S types are 0.08 ± 0.05 and 0.14 ± 0.08, respectively. Thus, although the two distributions clearly overlap, the S types tend to be slightly rougher than the C types, at least at centimeter-to-meter scales. This difference might exist because C-type material, which contains less metal and more volatiles than S-type material, is more fragile and more easily comminuted into fine-grained ("smooth") regolith.

Our values of μ_c for the S types decrease with asteroid size, suggesting some gravitational control of regolith generating processes. This result is qualitatively consistent with theoretical models (*5*), which predict thinner, rockier regoliths on smaller asteroids due to relatively inefficient retention of impact ejecta. For C types, the imprecision of our estimates precludes a reliable inference about how μ_c might depend on size.

Spectral shape: Large-scale structure. Our data also constrain surface properties at scales much larger than the radar wavelength, as follows. For objects with highly polarized echoes ($\mu_c \lesssim 0.1$), the shape of the OC echo spectrum is a function of the object's shape, the statistical distribution of surface slopes with respect to that shape, and the object's orientation. Among our targets, the one with the most reliably known dimensions is Pallas, for which stellar-occultation and optical-lightcurve data are well matched by an ellipsoid with axis lengths equal to 558, 526, and 532 km (*8*). Since Pallas is not terribly aspherical, it seems reasonable to approximate Pallas as a sphere and attempt to extract from the spectrum some constraints on surface slope statistics. However, the edges of the echo spectrum are obscured by noise, and therefore in order to progress we must either assume or estimate a value for the echo's bandwidth, B. For any rotating, rigid target, $B = (4\pi D \cos \delta)/\lambda P$, where P is the apparent rotation period, δ is the target-centered declination of the radar, and D is the breadth, measured normal to the line of sight, of

Table 1. Results from λ13-cm radar observations of mainbelt asteroids. Right ascension (RA), declination (DEC), and distance are given for epochs near the weighted midpoint of observation. Δf is the "raw" frequency resolution of our echo spectra, B_{EQ} the equivalent bandwidth (*3*) of the OC echo spectrum, σ_{oc} the OC radar cross section (*3*), μ_c the circular polarization ratio (of SC to OC echo power) (*3*), and $\hat{\sigma}_{oc} = 4\sigma_{oc}/\pi D^2$ the radar albedo (*17*), where the diameter D is derived from infrared radiometry (*18*) or, for Ceres (*11*), Pallas (*8*) and Metis (*12*), from timing stellar occultations.

Target	Taxonomic type	Midpoint of observations		RA (h)	DEC (deg)	Distance (AU)	Δf (Hz)	B_{EQ} (Hz)	σ_{oc} (km^2)	μ_c	Diameter (km)	$\hat{\sigma}_{oc}$
		Date*	Time (h)									
1 Ceres	C	84 Oct 28	4	3.42	9.1	1.86	19	1500	33000 ± 8700	0.04 ± 0.08	950	0.047 ± 0.018
2 Pallas	C	82 Mar 24	6	13.38	11.6	1.48	19	590	21000 ± 5400	0.05 ± 0.02	538	0.092 ± 0.024
4 Vesta	V	82 Feb 26	5	10.51	19.5	1.40	20	900	12000 ± 3100	0.40 ± 0.11	530	0.054 ± 0.021
5 Astraea	S	83 Mar 3	4	10.76	11.3	1.13	3	120	2400 ± 600	0.20 ± 0.04	121	0.21 ± 0.08
6 Hebe	S	85 Jan 20	3	5.98	8.8	1.39	19	600	4300 ± 1200	0.00 ± 0.12	204	0.13 ± 0.05
7 Iris	S	80 Sep 26	5	23.63	9.7	0.94	10	280	5900 ± 1500	0.08 ± 0.03	208	0.17 ± 0.06
8 Flora	S	81 Dec 8	4	6.06	18.0	0.98	20	220	1500 ± 380	0.16 ± 0.05	162	0.073 ± 0.027
9 Metis	S	84 Mar 20	4	12.15	8.7	1.44	10	180	3500 ± 920	0.18 ± 0.08	203	0.11 ± 0.03
12 Victoria	S	82 Oct 1	4	0.22	14.7	1.03	10	190	2100 ± 520	0.14 ± 0.03	135	0.15 ± 0.05
16 Psyche	M	80 Nov 19	5	5.16	18.2	1.70	20	540	14000 ± 370	0.14 ± 0.10	250	0.29 ± 0.11
19 Fortuna	C	82 Oct 1	6	1.42	9.8	1.08	19	550	3200 ± 820	0.04 ± 0.04	221	0.083 ± 0.031
41 Daphne	C	85 Apr 27	3	13.11	7.2	1.10	19	500	2900 ± 770	0.13 ± 0.08	203	0.090 ± 0.034
46 Hestia	P	82 Nov 13	5	3.69	16.2	1.26	19	110	900 ± 250	0.00 ± 0.11	131	0.067 ± 0.026
80 Sappho	S	83 Oct 28	4	2.18	14.6	0.91	10	77	650 ± 160	0.25 ± 0.05	83	0.12 ± 0.04
97 Klotho	M	81 Jan 30	4	8.09	7.9	1.23	10	45	1100 ± 320	no data	108	0.12 ± 0.05
139 Juewa	C	83 Feb 28	3	9.81	24.2	1.37	7	75	1300 ± 350	0.10 ± 0.10	172	0.056 ± 0.022
144 Vibilia	C	84 Oct 28	3	2.92	11.0	1.11	10	140	1800 ± 500	0.18 ± 0.10	131	0.13 ± 0.05
356 Liguria	C	83 Oct 28	2	1.42	18.0	1.23	10	72	1800 ± 460	0.12 ± 0.06	155	0.095 ± 0.036
554 Peraga	C	84 Oct 27	4	0.78	11.0	1.11	10	150	1600 ± 400	0.06 ± 0.06	101	0.20 ± 0.07
694 Ekard	C	83 Oct 29	2	0.06	17.0	1.00	10	170	610 ± 160	0.00 ± 0.10	101	0.076 ± 0.029

*Universal Time.

the target's polar silhouette. B cannot exceed $B_{max} = 4\pi D_{max}/\lambda P$, where D_{max} is the maximum breadth. For Pallas, D_{max} = 558 km and optical lightcurves (*9*) show that P = 7.811 hours, so B_{max} = 1980 Hz and B = 1980 cos δ. Since Pallas's half-power spectral bandwidth B_{HP} is about 500 Hz (Fig. 1), the constraint on the full bandwidth requires that $B_{HP}/B \gtrsim 0.25$. In contrast, lunar spectra are much more sharply peaked ($B_{HP}/B \lesssim 0.1$), and we infer that Pallas is much rougher than the Moon at scales no smaller than several meters. A useful measure of large-scale roughness is the rms value, s_0, of the surface slope distribution. Since $s_0 \sim 6°$ for the moon (*10*), Pallas's value must be much larger.

We have estimated s_0 and B for Pallas by fitting to the spectrum a model derived for a sphere whose backscattering law has the form: $(d\sigma/dA) \sim G \exp(-G \tan^2\theta) / \cos^4\theta$, where dA is an element of surface area, θ is the angle between the line of sight and the normal to dA, and $s_0 = G^{-1/2}$ radians (*10*). This law, which assumes that the surface height distribution and lateral autocorrelation function are Gaussians, has been used previously to interpret radar echoes from Mars and the Moon. For Pallas, the least-squares solution yields a statistically acceptable model (the barely visible dashed curve in Fig. 1) with parameter estimates and standard errors: B = 1100 ± 80 Hz and s_0 = 27° ± 3°. The bandwidth estimate corresponds to δ = 56° ± 3°, in adequate agreement with constraints (*9*) on Pallas's pole direction derived from optical lightcurves.

Occultation data yield preliminary estimates of D_{max} equal to 950 km for Ceres (*11*) and 230 km for Metis (*12*). We combine these results with tabulated rotation periods (*13*) to obtain estimates of B_{max} equal to 2900 Hz and 1300 Hz, respectively. Our Ceres spectrum has a half-power bandwidth of ~1500 Hz, so $B_{HP}/B \gtrsim 0.5$. Since $B_{HP}/B \approx 0.45$ for our Pallas model spectrum, root-mean-square slopes probably are at least as large on Ceres as they are on Pallas. For Metis, $B_{HP} << B_{max}$. This relation is presumably due to a nearly pole-on view, an orientation suggested by the low amplitudes of optical lightcurves (*14*) obtained during several months bracketing the radar runs.

Lacking occultation data for our other 17 targets, we approximate D_{max} with $10^{0.4\Delta m} D$, where D is the radiometric diameter in Table 1 and Δm is the target's maximum observed peak-to-valley

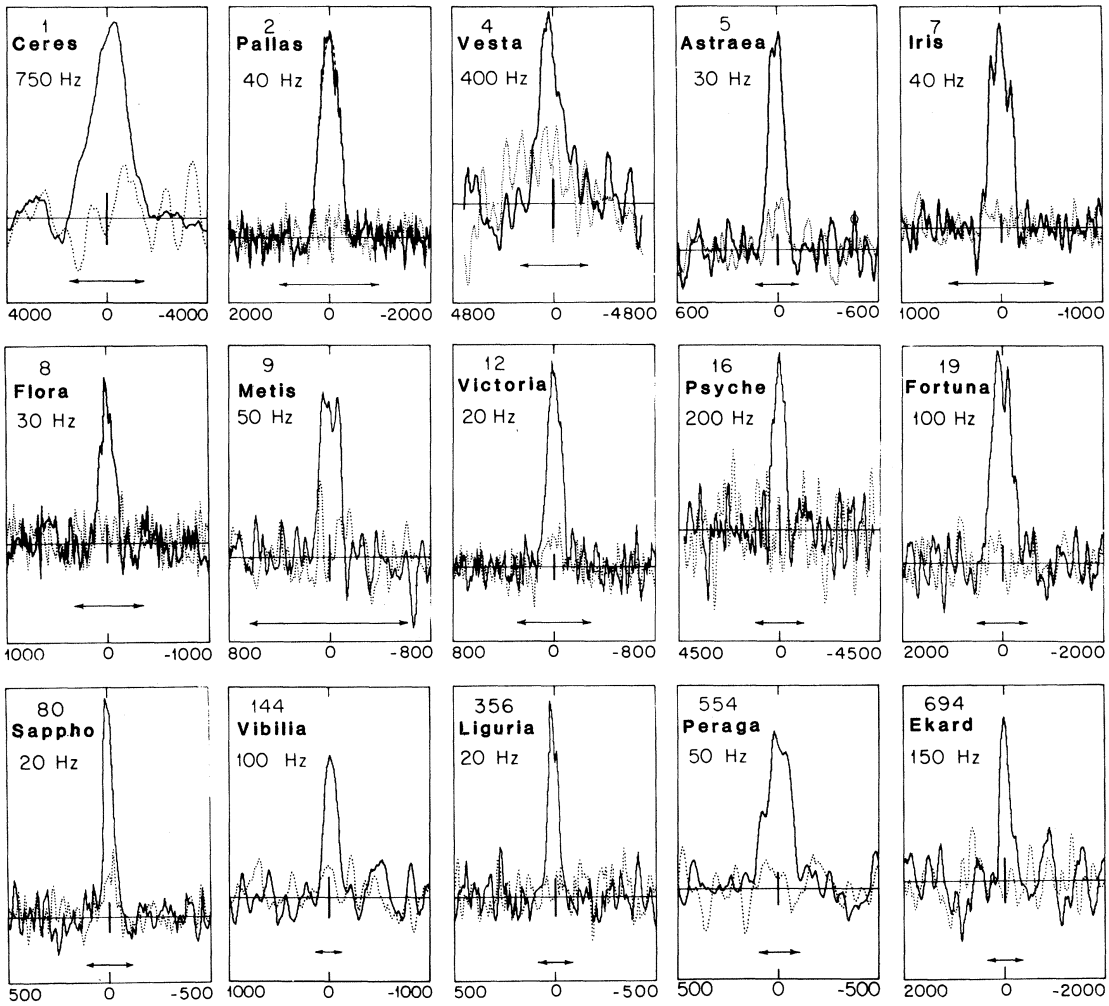

Fig. 1. Radar echo spectra obtained in the OC and SC polarizations (solid and dotted curves, respectively), filtered to the indicated frequency resolution. Echo power density is plotted against Doppler frequency. Central vertical bars represent ±1 standard deviation of the receiver noise. Horizontal arrows show the maximum value, B_{max}, expected for the full spectral bandwidth, B.

lightcurve amplitude in magnitudes (*13*). Further, we use tabulated rotation periods (*13*) for our calculation of B_{max}, as indicated by horizontal arrows in Fig. 1. Although detailed analyses must await refined determinations of these targets' dimensions and pole directions, the available information suggests that each asteroid has $B_{HP}/B > 0.2$. Each target thus appears to be substantially rougher than the Moon at some scale that, given our low-to-moderate values of μ_c, must be no smaller than several meters. Whereas various degrees of decimeter-scale roughness certainly exist on our targets, the surface component responsible for most of the echo power and for the broad shapes of our OC spectra must be very smooth at centimeter-to-meter (that is, "human") scales and must be very rough (that is, must have very large rms slopes) at some much larger, "topographic" scale.

A likely candidate for the source of the large-rms-slope component of asteroid surfaces is hypervelocity impact cratering. Theoretical calculations (*15*) suggest that the weak gravity fields and small radii of curvature of asteroid surfaces will cause impact processes on these objects to be intrinsically different from those on planet-sized bodies. For example, very energetic impacts could generate severe antipodal and overall surface modification effects. The precise scales of impact-produced structure on asteroids are difficult to predict theoretically, but they might be enormous compared to the minimum roughness scale (several meters) needed to satisfy the radar measurements. Major topographic relief on asteroids is, in fact, evident in results from timing stellar occultations (*8, 17*), in the form of kilometer-scale differences between measured positions of points on the asteroid limbs and the predictions from elliptical-limb models.

Albedo: Density, porosity, and metal content. A useful measure of radar reflectivity is the OC radar albedo, $\hat{\sigma}_{oc} \equiv \sigma_{oc}/A_p$, where A_p is the target's projected area. Our albedo estimates (*17*) are given in Table 1 and plotted as a function of infrared radiometric (*18*) or stellar occultation diameter in Fig. 2b. They range from 0.047 to 0.29 and have an unweighted mean and rms dispersion of 0.12 ± 0.06. Corresponding statistics for C types (0.10 ± 0.04) and S types (0.14 ± 0.04) quantify our impression from Fig. 2b that, whereas the C and S albedo distributions are broad and overlap each other, S types tend to be marginally brighter, on average, than C types. No simple dependence of $\hat{\sigma}_{oc}$ on size is evident.

To interpret these results physically, we write $\hat{\sigma}_{oc} = gR$, where R is the Fresnel power reflection coefficient for normal incidence and the backscatter gain g depends on the target's angular scattering law, shape, and orientation. For a smooth sphere, $g = 1$. For a sphere scattering according to the Gaussian law fit to the Pallas spectrum, $g = 1.1$. We are unaware of any rough-surface scattering law compatible with low values of μ_c and yielding $g > 1.5$ for a sphere (or for an ellipsoid with axis ratios $\lesssim 2$ when observations are averaged over many orientations), and it seems that R rather than g must be responsible for most of the variance in $\hat{\sigma}_{oc}$. For dry, particulate mixtures of rock and metal with particle sizes $\lesssim \lambda/100$, R depends strongly on the bulk density, d (*19*). Bulk density, in turn, is a function of the porosity (p), the metal weight fraction (w), and the specific gravities (d_r, d_m) of the rock and metal phases.

C- and P-type objects are thought to resemble carbonaceous chondrites (*7*), for which $w \lesssim 0.05$ (*20*), so most of the variance in these objects' albedos probably arises from variations in d_r or p. Since lunar soil has $w \approx 0$ (*21*), comparison of the Moon's albedo (0.07) with those estimated for C and P types suggests that these asteroids' surfaces have bulk densities comparable to or slightly larger than lunar values.

S- and M-type asteroids have VIS/IR reflection spectra that strongly suggest the presence of free metal and several common silicates, but the metal abundances are uncertain (*22*). Hence, we do not know (i) whether S types are mineralogically more akin to stony iron meteorites ($0.4 \lesssim w \lesssim 0.6$) or to ordinary chondrites ($w \lesssim 0.2$), and (ii) whether M types are more akin to irons ($w > 0.9$) or to enstatite chondrites ($w \lesssim 0.3$). Irons and stony irons are igneous rocks, whereas chondrites are primitive assemblages of solar nebular condensates and have never been heated to temperatures near their melting points. Identification of the parent bodies of these different meteorite types would permit important insights into chemical and thermodynamic conditions during the earliest stages of planetary formation (*22*).

How can our radar albedo estimates constrain the metal abundances and possible meteoritic analogues of our targets? Let us assume that our albedos provide unbiased estimators for R (*23*); that $R = R(d)$, as discussed above; and that "typical" values ($d_m = 7.8$, $d_r = 3.2$) pertain for the specific gravities of meteoritic metal and rock. Then contours of constant d and R in the (w,p) plane are straight lines, as in Fig. 3; thus, this figure provides a joint constraint on porosity and metal abundance for each of our targets. R is more sensitive to porosity than to metal concentration, and therefore any inference of w (and hence of meteoritic association) depends on assumptions about p. Porosity depends on grain shape and size distributions and on grain arrangement, which depends on

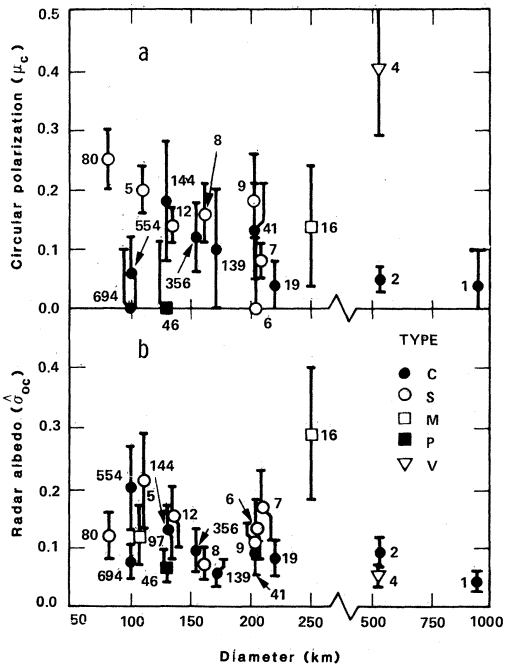

Fig. 2. Estimates of circular polarization ratio (μ_c) and radar albedo ($\hat{\sigma}_{oc}$), plotted against asteroid diameter.

interparticle forces and on the emplacement process itself. Estimates of p for lunar soils (*24*) range from 0.3 to 0.7, but nearly all fall between 0.35 and 0.55, in agreement with a large variety of theoretical and empirical investigations (*25*) of particle-packing phenomena.

From Fig. 3, we see that our highest albedo estimate, 0.29 ± 0.11 for asteroid 16 Psyche, is consistent with a nearly entirely metallic composition and porosities (~0.4 to ~0.5) that seem quite ordinary. This albedo is also consistent with enstatite-chondritic metal abundances (≲0.3) and porosities (≲0.2) that are much lower than lunar values, but we consider such low porosities unlikely on several grounds. First, grain size distributions in chondrites are depleted in fractions of smaller size relative to distributions in lunar soils and breccias (*26*), and porosity usually increases as the size distribution narrows (*25*). Second, gravitational compaction of regolith should be much less effective on Psyche than on the moon. Finally, naturally occurring or industrially produced powders rarely, if ever, have porosities as low as 0.2 (*25*). These considerations prompt us to favor the high-w interpretation of Psyche's radar albedo. If this interpretation is correct, Psyche might be the collisionally stripped, metallic core of a differentiated asteroid and, by far, the largest piece of "refined" metal in the solar system. On the other hand, our only other M type, 97 Klotho, has an albedo estimate that is consistent with typical lunar porosities and essentially any metal concentration. By the same token, our S-type albedos can be explained by either (i) stony iron metal abundances and typical lunar porosities, or (ii) ordinary chondritic metal abundances and porosities near the low extreme of lunar values.

Conclusions. Our radar observations suggest wide variations in metal abundance, porosity, and decimeter-scale roughness on mainbelt asteroid surfaces, underscoring the diversity of the asteroid population already evident from VIS/IR studies. Additional observations are expected to double our current sample size within a few years, and should help to clarify the distributions of asteroid radar albedos and polarization ratios as well as the extent to which those properties are correlated with size and composition.

Although the radar signatures of mainbelt asteroids require substantial surface roughness at some scale much larger than a meter, we cannot discern the precise scale of this structure, much less the actual morphologies of surface features. Similarly, our radar albedos bolster the hypothesis that metal concentrations on asteroids span the gamut, but serious questions remain about detailed mineralogies, meteoritic associations, and evolutionary histories, especially for the enigmatic S types. Spacecraft reconnaissance of a representative sample of mainbelt asteroids could resolve many of these issues and would furnish benchmarks to guide the interpretation of ground-based observations. A critical first step in this direction is anticipated for December 1986, with a flyby of the S-type asteroid 29 Amphitrite by the Galileo spacecraft (*27*).

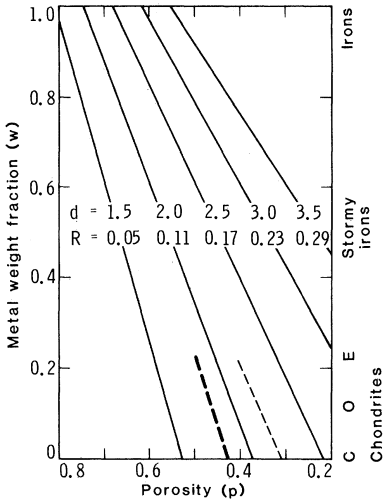

Fig. 3. Reflection coefficient (R) of particulate mixtures of rock and metal. Metal weight fraction (w) is plotted as a function of porosity (p) for five values of R and bulk density (d). We assume specific gravities d_m equal to 7.8 for metal and d_r equal to 3.2 for rock. Heavy and faint dashes show the d equal to 2.0 line for d_r equal to 3.5 and 2.9, respectively. Typical values of w for iron meteorites, stony irons, and the three chondrite classes (enstatite, ordinary, carbonaceous) are indicated. We assume an empirical relation, $R(d) = 0.12d - 0.13$, derived from measurements (*19*) of the radar-frequency electrical properties of powders containing no particles larger than 1 mm. Values of R estimated for powders satisfying $1.5 \leq d \leq 3.5$ and $w < 0.9$ are within 0.02 of this approximation.

References and Notes

1. R. F. Jurgens and R. M. Goldstein, *Icarus* **28**, 1 (1976). Asteroids are identified by a number and a name.
2. S. J. Ostro, D. B. Campbell, I. I. Shapiro, *Astron. J.* **88**, 565 (1983).
3. Radar cross section equals 4π times the backscattered power per steradian for unit incident flux at the target. Uncertainties assigned to radar cross sections are the root sum square of systematic (that is, calibration) errors, estimated as 25 percent of the cross-section values, and the standard deviation of the receiver noise in the equivalent bandwidth (B_{EQ}; see Table 1) of the OC echo spectrum. By definition [M. E. Tiuri, *IEEE Trans. Antennas Propag. AP-12*, 930 (1964)], $B_{EQ}/\Delta f = (\Sigma S_i)^2/\Sigma S_i^2$, where the S_i are the spectral elements. For our targets, the SC equivalent bandwidth is lower than the OC value. The standard deviations quoted for μ_c propagate from the receiver noise alone, as discussed in (*2*, Appendix I).
4. J. V. Evans and T. Hagfors, *J. Geophys. Res.* **71**, 4871 (1966).
5. K. R. Housen and L. L. Wilkening, *Annu. Rev. Earth Planet. Sci.* **10**, 355 (1982).
6. D. J. Tholen, thesis, University of Arizona, Tucson (1984).
7. J. Gradie and E. Tedesco, *Science* **216**, 1405 (1982); C. R. Chapman, *Rev. Geophys. Space Phys.* **21**, 196 (1983).
8. L. H. Wasserman *et al.*, *Astron. J.* **84**, 259 (1979).
9. R. P. Binzel, *Icarus* **59**, 456 (1984).
10. R. A. Simpson and G. L. Tyler, *IEEE Trans. Antennas Propag.* **AP-30**, 438 (1982).
11. W. B. Hubbard *et al.*, *Lunar Planet. Sci. Conf. 16 Abstr.* (1985), p. 370.
12. L. K. Kristensen, personal communication.
13. A. W. Harris and J. W. Young, *Icarus* **54**, 59 (1983).
14. K. W. Ziegler and W. B. Florence, *Bull. Am. Astron. Soc.* **16**, 691 (1984).
15. M. J. Cintala, J. W. Head, J. Veverka, *Proc. Lunar Planet Sci. Conf.* **9**, 3803 (1978).
16. R. L. Millis *et al.*, *Icarus* **61**, 124 (1985).
17. Our calculation of errors in OC "radar albedo," $\hat{\sigma}_{oc} \equiv 4\ \sigma_{oc}/D^2$ follows Appendix I of (*2*) and requires error estimates for σ_{oc} and D. For σ_{oc}, we assumed the errors in Table 1. For D, we assumed fractional errors equal to 0.02 for Pallas, 0.05 for Ceres and Metis, and 0.1 for the other targets. The radar albedo should not be confused with the "geometric albedo," which equals $(1 + \mu_c)\ \hat{\sigma}_{oc}/4$.
18. D. Morrison and B. Zellner, in *Asteroids*, T. Gehrels, Ed. (Univ. of Arizona Press, Tucson, 1979), pp. 1090–1097; R. H. Brown, D. Morrison, C. M. Telesco, W. E. Brunk, *Icarus* **52**, 188 (1982).
19. S. J. Ostro and W. B. Westphal, unpublished results.
20. R. T. Dodd, *Meteorites* (Cambridge Univ. Press, Cambridge, 1981), pp. 19, 309–328; V. F. Buchwald, *Handbook of Iron Meteorites* (Univ. of California Press, Berkeley, 1975), p. 62.
21. J. I. Goldstein and H. Yakowitz, *Proc. Second Lunar Sci. Conf.* **1**, 177 (1971).
22. M. J. Gaffey, *Icarus* **60**, 83 (1984); M. A. Feierberg, H. P. Larson, C. R. Chapman, *Astrophys. J.* **257**, 361 (1982); J. T. Wasson and G. W. Wetherill, in *Asteroids*, T. Gehrels, Ed. (Univ. of Arizona Press, Tucson, 1979), pp. 926–974.
23. Since $R = \hat{\sigma}_{oc}/g$ by definition and we expect g to exceed unity by ~10 percent, the assumption that $R = \hat{\sigma}_{oc}$ probably causes some overestimation of R. A similar bias in R would result if part of the OC echo arose from decimeter-scale roughness or multiple scattering, a likely possibility for targets with large μ_c. Underestimation of R might result if the regolith density near the surface were not constant, but instead increased gradually down to some depth $\gtrsim\lambda/4$. As discussed by R. A. Simpson [*Proc. IEEE Trans. Antennas Propag.* **AP-24**, 17 (1976)], this configuration could create an impedance match between the asteroid and free space, severely attenuating R. The presence of metal, which has high dielectric loss, in transition layers could cause similar effects.
24. W. D. Carrier III, J. K. Mitchell, A. Mahmood, *Proc. Lunar Sci. Conf.* **4**, 2403 (1973).
25. W. A. Gray, *The Packing of Solid Particles* (Chapman and Hall, London, 1968), pp. 43–107; G. P. Bierwagen and T. E. Saunders, *Powder Technol.* **10**, 111 (1974); R. J. Wakeman, *ibid.* **11**, 297 (1975); M. J. Powell, *ibid.* **25**, 45 (1980); G. Herdan, *Small Particle Statistics* (Academic Press, New York, 1960), pp. 184–191.
26. S. K. Bhattacharya, J. N. Goswami, D. Lal, P. Patel, M. N. Rao, *Proc. Lunar Sci. Conf.* **6**, 3509 (1975).
27. *NASA Activities* **16**, 3 (1985).

28. We thank the Arecibo Observatory staff for help with the observations, A. Forni for preparing the ephemerides, A. Ferro for programming assistance, and K. Banwart and C. Ikuta for secretarial assistance. Part of this research was conducted at the Jet Propulsion Laboratory, California Institute of Technology, under contract with the National Aeronautics and Space Administration, and part was supported by NASA grant NAGW-116 and NSF grant PHY-84-09671. The Arecibo Observatory is part of the National Astronomy and Ionosphere Center which is operated by Cornell University under contract with the National Science Foundation and with support from NASA.

22 April 1985; accepted 27 June 1985